Origin of an Isothermal *R*-Martensite Formation in Ni-rich Ti-Ni Solid Solution: Crystallization of Strain Glass

Yuanchao Ji,[1,*] Dong Wang,[1] Xiangdong Ding,[1,†] Kazuhiro Otsuka,[2] and Xiaobing Ren[1,2,‡]

[1]*Frontier Institute of Science and Technology and State Key Laboratory for Mechanical Behaviour of Materials,*
Xi'an Jiaotong University, Xi'an 710049, China
[2]*Ferroic Physics Group, National Institute for Materials Science, Tsukuba, 305-0047 Ibaraki, Japan*

We report that R martensite isothermally forms with time in a solution-treated $Ti_{48.7}Ni_{51.3}$ single crystal. This abnormal formation originates from the growth of a short-range ordered R phase with time, i.e., the "crystallization" of strain glass. The established time-composition-temperature Ti-Ni diagram shows a time evolution of the R phase and composition-temperature phase diagram. The presence or absence of the R phase in this new diagram, as well as in other conditions (like doping Fe or aging), is explained in a unified framework of free-energy landscape. Our finding suggests a new mechanism for the isothermal martensite formation, which could be applied to other metal and ceramic martensitic systems to find new phases and novel properties.

Time plays a crucial role in diffusional transformations because of their occurrence through atomic migration or diffusion [1–3]. Different kinds of microstructures and metastable phases may appear with the time evolution, which have been used to achieve desired physical properties of materials (steel is the best known example [2]). On the other hand, time independence is a primary characteristic of martensitic or diffusionless transformations because they occur through a cooperative movement of many atoms with a velocity of sound [1–3]. However, the nucleation process is a time-dependent one (creating the so-called incubation time), and results in isothermal martensitic transformations when the incubation time is long enough for experimental measurements (denoted as the nucleation-controlled isothermal martensite formation) [1,3–10]. Nevertheless, it is believed that time is not essential for achieving a stable phase and determining a diffusionless equilibrium phase diagram, because the rapid transformation rate in the growth process provides little time window for the existence of metastable states. In this Letter, however, we report a surprising discovery, a normally "nonexistent" martensite isothermally appears through a gradual growth with time (denoted as the growth-controlled isothermal martensite formation). This provides evidence for the existence of time-dependent phase evolution in martensitic systems.

Ti-Ni alloy (nitinol), the prototype of shape memory alloys and the most commonly used one since its discovery in the early 1960s, undergoes a martensitic transition from the $B2$ (ordered body-centered-cubic) phase to the $B19'$ (monoclinic) phase, which gives rise to the shape memory effect and superelasticity [11,12]. Besides $B2$ austenite and $B19'$ martensite, another R (trigonal) martensite sometimes appears through alloying (doping a third element like Fe),

aging (forming fine precipitates) or cold rolling (generating a high density of dislocations) to the Ti-Ni solid solution [11,12]. However, R martensite is known to be nonexistent in solution-treated binary Ti-Ni alloys [11–15].

In the following, we show that in a solution-treated binary $Ti_{48.7}Ni_{51.3}$ alloy, R martensite, which is expected to be nonexistent under such conditions, forms with time. This isothermal R martensite arises from the growth of a short-range ordered (SRO) R phase (i.e., crystallization of strain glass). The gradual R-martensite formation can be understood under the framework of a frustrated Landau free-energy landscape, and it also explains why R-martensite forms in various conditions like Fe doping, etc.

All samples were cut from a $Ti_{48.7}Ni_{51.3}$ single crystal, and then solution-treated at 1273 K for 1 h followed by water quench. Transition behavior was conducted using differential scanning calorimetry DSC (Q200 TA Instruments) with a cooling or heating rate of 10 K/min. Electrical resistivity was studied during an isothermal dwelling at 193.1 K by a four-probe method with a constant current of 100 mA. *In situ* x-ray diffractometry using Shimadzu XRD7000 was performed to detect the structural change with time. Mechanical susceptibility was measured on a dynamic mechanical analyzer DMA (Q800 from TA Instruments) using a step cooling or heating method with a single cantilever mode in the frequency range from 0.1 to 10 Hz.

We first demonstrate that a new phase (later determined as R martensite) forms with time. Figure 1(a) shows that the normal $B2$–$B19'$ martensitic transition occurs in a solution-treated $Ti_{48.7}Ni_{51.3}$ single crystal, appearing as an enthalpy peak or dip in the DSC curve. The transition temperatures are determined to be approximately $M_s (\sim 178.6 \text{ K})$, $M_f (\sim 155.0 \text{ K})$, $A_s (\sim 201.4 \text{ K})$, and $A_f (\sim 223.8 \text{ K})$. The ideal thermodynamic phase transition temperature (i.e., the
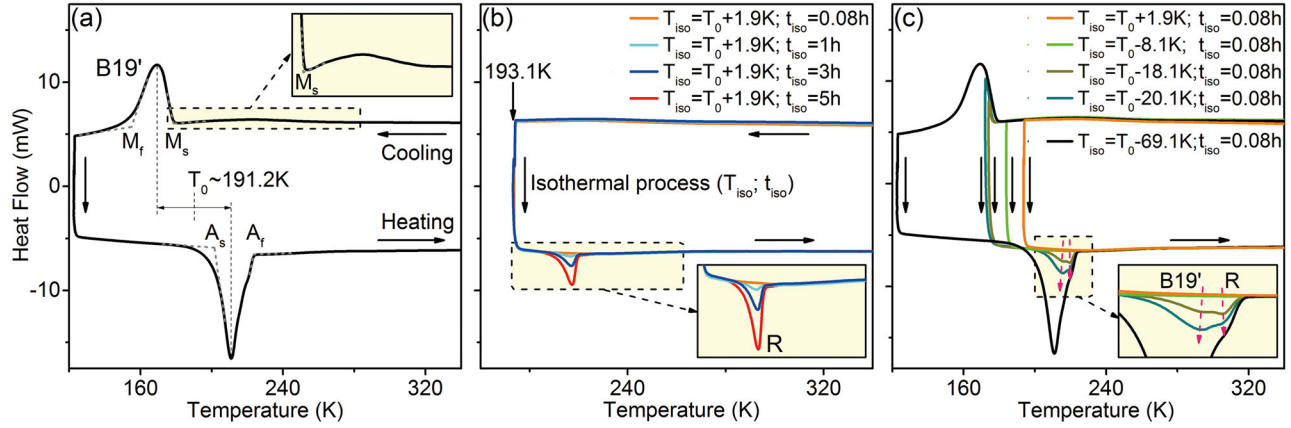
FIG. 1 (color online). (a) The DSC result shows the occurrence of the $B2$–$B19'$ martensitic transition, whose ideal transition temperature is estimated as the middle point between the peak and dip temperature ($T_0 \approx 191.2$ K). M_s, M_f, A_s, and A_f represent the martensite start temperature, the martensite finish temperature, the reverse transformation start temperature, and the reverse transformation finish temperature, respectively. Note that there exists a board hump above M_s (see the inset). (b) A series of DSC experiments with different isothermal aging time (t_{iso}) at 193.1 K (T_{iso}) reveal the formation of a new phase (later determined as R martensite) during the isothermal aging process. (c) Another series of DSC experiments by changing T_{iso} while keeping the same isothermal aging time. With lowering T_{iso}, DSC heating curves show two dips: the first becomes larger and shifts to the corresponding reverse $B19'$ martensitic transition one; the second corresponds to the unknown phase as shown in (b).

temperature where the austenite and martensite have the same free energy) is calculated by averaging the peak (cooling) and dip (heating) temperatures $T_0 \approx (170.4 + 212.0)/2 = 191.2$ K instead of $T_0 = (A_s + A_f + M_s + M_f)/4$, because A_f is not exactly the finishing temperature of the $B19'$ martensite [see Fig. 1(c)]. It is noticeable that a broad hump appears prior to the $B2 \rightarrow B19'$ transition [inset of Fig. 1(a)], which indicates the occurrence of another transition [16]. To identify its nature, we performed a series of isothermal DSC experiments at 193.1 K ($T_{iso} = T_0 + 1.9$ K) for different lengths of isothermal aging time (t_{iso}). Figure 1(b) shows that a similar broad hump exists in both cooling and heating processes at the shortest isothermal aging time ($t_{iso} = 0.08$ h). However, an endothermic dip appears upon heating and becomes more enhanced with increasing aging time t_{iso} [inset of Fig. 1(b)], which implies the gradual formation of a new phase during the isothermal aging process. To distinguish the new phase from $B19'$ martensite, we designed another series of DSC experiments by changing T_{iso} [Fig. 1(c)]. For T_{iso} above the starting temperature of $B19'$ martensite (M_s), the DSC curve of $T_{iso} = T_0 - 8.1$ K exhibits a similar and complete hump as compared with that of $T_{iso} = T_0 + 1.9$ K. However, for T_{iso} below M_s, DSC curves upon heating do not show the expected single dip (i.e., reverse $B19'$ transition) but two dips. The first dip upon heating becomes more enhanced and shifts towards the reverse transition dip of $B19'$ martensite with decreasing T_{iso}. The temperature range of the second dip essentially overlaps with that of the isothermal one in Fig. 1(b), and its formation can be roughly understood by the time-temperature equivalence principle [17]: reducing the temperature lead to increasing the driving force and thus accelerating the transformation

process, which is equivalent to increasing transformation time at constant temperature.

We then tried two methods to identify the structure of this new phase. First, it is known that electrical resistivity is a sensitive probe to detect a phase transformation, and it is more powerful in Ti-Ni alloys because (i) the resistivity of $B2$ austenite is higher than that of $B19'$ martensite, but lower than that of R martensite, and (ii) both $B2$ austenite and $B19'$ martensite have a positive temperature coefficient of resistivity, whereas R martensite has a negative one [11–16,18]. Figures 2(a) and 2(b) show the variation of relative resistivity with isothermal aging time. The gradual increase of resistivity during the isothermal aging indicates
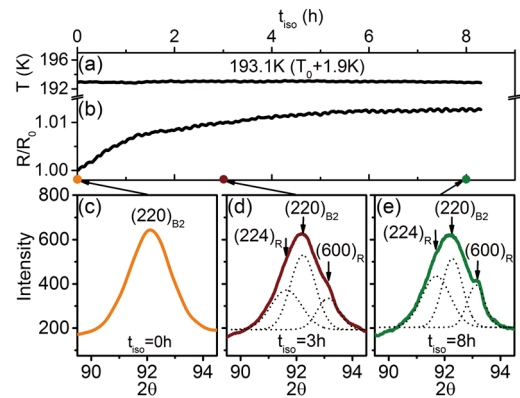

FIG. 2 (color online). (a) Temperature monitor of the isothermal aging experiment, and (b) increase of electrical resistivity during isothermal aging, which reveals the formation of R martensite. (c), (d), and (e) Time dependence of *in situ* x-ray diffraction patterns. Additional peaks gradually appear close to $(220)_{B2}$ peak and are determined to be the $(224)_R$ and $(600)_R$.

the R-martensite formation, because (i) the phase with higher resistivity as compared with $B2$ austenite must be R martensite and (ii) according to the previously mentioned time-temperature equivalence principle, the resistivity increase with time corresponds to the resistivity increase with lowering temperature (i.e., a negative temperature resistivity coefficient). Second, we directly detected the structure change during the isothermal process by x-ray diffraction (XRD) measurements. *In-situ* XRD experiments with time at 193.1 K($T_0 + 1.9$ K) [Figs. 2(c), 2(d), and 2(e)] show that additional diffraction peaks gradually appeared adjacent to the $(220)_{B2}$ peak and were determined to be the $(224)_R$ and $(600)_R$, respectively [12,19]. Therefore, from the above two methods, the new phase formed during isothermal aging at 193.1 K is uniquely determined to be R martensite.

To reveal the underlying mechanism of the gradual R-martensite formation, a mechanical susceptibility measurement was used according to previous studies [16]. Figure 3(a) shows temperature-dependent DMA curves of the storage modulus and the associated internal friction (mechanical loss). With decreasing temperature, the elastic modulus continues softening and reaches a minimum at $\sim$194 K, accompanied by a peak of internal friction.

These features clearly indicate the occurrence of a phase transition, consistent with the hump in the DSC curve [inset of Fig. 1(a)]. Furthermore, the dip temperature (T_g) shows a frequency dependence; i.e., it shifts to a lower temperature with lowering frequency, and this frequency dispersion follows the Vogel-Fulcher relation [inset of Fig. 3(a)]. These features are characteristics of the previously reported strain glass transition [13–16,18]. With subsequent cooling, the $B19'$ formation is revealed by the appearance of another peak in internal friction and the frequency-dependent shrinking of the storage modulus.

Next, we designed a series of isothermal DMA experiments to provide a direct link between the R-martensite formation and strain glass transition. Figure 3(b1) shows cooling curves, all passing T_g (i.e., occurrence of the strain glass transition). Figure 3(b2) shows that upon heating the $R \rightarrow B2$ transition occurs at $\sim$218 K after an isothermal aging process in the strain glass state, and this transition becomes more pronounced with lowering T_{iso} (manifested by the larger change in storage modulus and the higher peak of internal friction), which agree well with DSC results in Figs. 1(b) and 1(c). Therefore, these results indicate that the long-range ordered (LRO) R phase originates from a gradual growth of SRO R-phase domains in the strain glass state [13–16] during the isothermal or cooling process. This aging-induced glass-to-LRO phase transition is very similar to the crystallization of chemically disordered glasses [17].

Based on the above results, a time-temperature-transformation (TTT) diagram of the isothermal R-martensite formation is shown in Fig. 4(a); such a diagram is commonly used to characterize an isothermal transition. The TTT diagram shows that the LRO or equilibrium R martensite stems from a SRO strain glass state. This process is analogous to the formation of crystal from a chemically
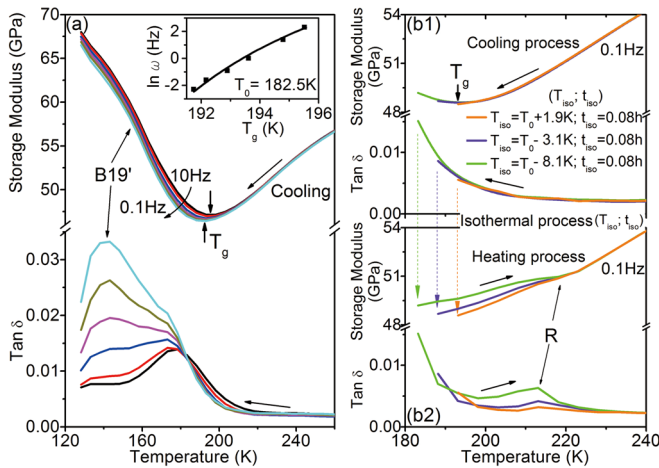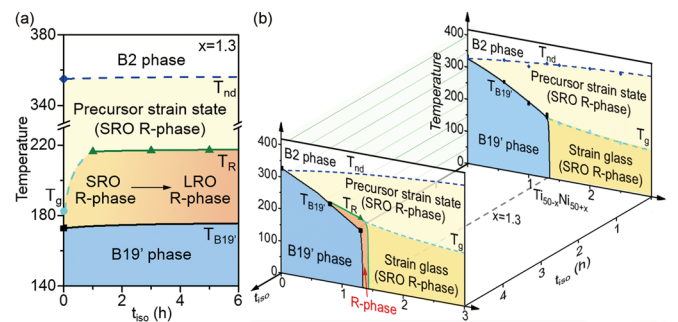

FIG. 3 (color online). (a) DMA results show that the dip of the storage modulus (at $T_g \sim 194$ K) and the associated peak of internal friction exhibit a frequency dependence, which follows the Vogel-Fulcher relation $\omega = \omega_0 \exp[-E_a/k_B(T_g - T_0)]$ (the inset), where ω is the frequency, ω_0 the frequency prefactor, E_a the activation energy, k_B the Boltzmann constant, T_g the strain glass freezing temperature, and T_0 the ideal freezing temperature. They are characteristics of a strain glass transition. Upon subsequent cooling, the $B19'$ martensite forms as indicated by another peak in the internal friction and weak frequency dependence of the storage modulus. (b1) and (b2) A series of isothermal DMA experiments with different T_{iso}. Strain glass transition occurs upon cooling [(b1)]; the growth of SRO R-strain-glass domains into a LRO R phase during the isothermal process gives rise to a $R \rightarrow B2$ transition upon heating, which results in a more pronounced $R \rightarrow B2$ transition with lowering T_{iso} [(b2)].

FIG. 4 (color online). (a) Time-temperature-transformation (TTT) diagram of $Ti_{48.7}Ni_{51.3}$. T_{nd}, T_R, T_g, and $T_{B19'}$ denote the nanodomain formation temperature, R-phase formation temperature, strain glass transition temperature, and $B19'$ phase formation temperature, respectively. (b) Time evolution of the Ti-Ni (solution-treated) phase diagrams. The two cross sections ($t_{iso} = 0$ h and $t_{iso} = 5$ h) correspond to the Ti-Ni phase diagram without and with isothermal aging, respectively. The phase diagram at $t_{iso} = 0$ h is cited from Ref. [15].

disordered glass during isothermal aging, known as crystallization of glass [17].

With the discovery of isothermal R martensite, the previous Ti-Ni (solution-treated) phase diagram [15] needs to be modified to include this new equilibrium phase, as shown in Fig. 4(b). The previous phase diagram can be viewed as a cross section of aging time $t_{iso} = 0$ h, where there are four different states: the $B2$ phase, $B19'$ phase, precursor strain state, and strain glass state, the latter two of which exhibit SRO R-phase symmetry [15]. With increasing isothermal aging time R phase appears between the SRO R phase and $B19'$ phase and the new phase diagram corresponds to the cross section of $t_{iso} = 5$ h, which resembles the Ti-Ni-Fe phase diagram but shows much narrower R-phase regime [18]. More detailed investigations show that the lower composition limit for the appearance of isothermal R phase is around 50.8 at.% Ni and the upper limit is around 51.5 at. % Ni [20]. Based on this equilibrium phase diagram, R-phase like signatures of both the precursor strain state and strain glass state can be understood as a reminiscence of the $B2$-R phase transition, which clearly excludes the effect of $B19'$ martensite (i.e., no SRO $B19'$ phase).

Next, we provide a qualitative explanation for the intriguing isothermal appearance of the "nonexistent" R martensite in solution-treated binary Ti-Ni alloys, as well as the R-martensite formation by doping third elements (e.g., Fe) or producing precipitates. Generally speaking, these seemingly different results arise from a common source: the competition between (i) the thermodynamic driving force for the R-martensite formation, and (ii) the kinetic slowing down of the R-martensite formation due to the frustration of dopants (excess-Ni, Fe) or precipitates [12–16]. The strength of these two factors determines the presence or absence of R martensite. Figure 5 shows four types of free energy landscapes for the martensitic transition from $B2$ to $B19'$ via an intermediate R martensite, where the relative stability of $B2$, R, and $B19'$ is based on experimental results and first-principles calculations [11–15,21,22]. (I) Figure 5(a) shows the free energy landscape of Ti$_{50}$Ni$_{50}$ (ideally with no dopants), where R martensite is a metastable phase with low stability and its kinetic slowing down is absent. Upon cooling, $B2$ transforms directly to $B19'$, without stopping at R martensite (path a of $B2$-$B19'$). (II) Figure 5(b) shows the free energy landscape of Ti$_{48.7}$Ni$_{51.3}$, where excess-Ni dopants produce (i) an increased thermodynamic stability of R martensite relative to $B2$ and $B19'$ [12,22] as illustrated by a deepening of the R energy well and (ii) a slowing down of the kinetics (because the formed strain glass has very slow dynamics [14]). At temperature T_1 where the kinetic energy $k_B T_1$ is slightly lower than local barriers (dotted red line) created by excess Ni, R martensite cannot appear immediately because the system is trapped among local barriers (i.e., a strain glass state). After the isothermal aging, the system has
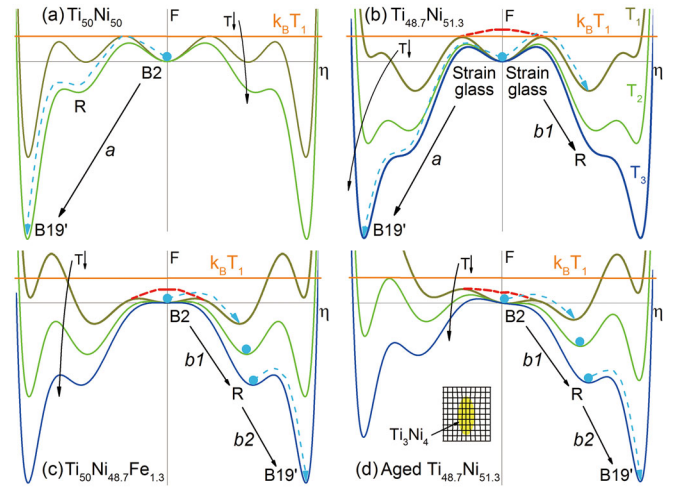

FIG. 5 (color online). Free-energy landscapes of the $B2$–$B19'$ martensitic transition via an intermediate R phase. (a) For Ti$_{50}$Ni$_{50}$, the $B2$ phase transforms directly to the $B19'$ phase (path a of $B2$-$B19'$). (b) For Ti$_{48.7}$Ni$_{51.3}$, at temperature T_1 where the kinetic energy $k_B T_1$ is slightly lower than local barriers (dotted red line), the isothermal R phase can be formed [Fig. 1(b)] through providing sufficient time to overcome local barriers (in a strain glass state). When the temperature is slightly lower than M_s (e.g., T_2), both the R phase and the $B19'$ phase appear [Fig. 1(c)] due to the increase of both the R and $B19'$ driving forces. When the temperature is much lower than M_s (e.g., T_3), the $B19'$ phase becomes the most stable phase, thereby leading to the normal transformation path a of strain glass $B19'$ [Fig. 1(a)]. (c) For Ti$_{50}$Ni$_{48.7}$Fe$_{1.3}$, the Fe dopant, strongly stabilizing R phase while creating weaker local barriers, gives rise to the transformation path $b1$ of $B2$-R under continuous cooling. (d) For precipitate-containing Ti$_{48.7}$Ni$_{51.3}$, the R-phase transition also occurs since precipitates (i.e., Ti$_3$Ni$_4$, inset) have similar effects as the Fe dopant.

sufficient time to go out of the local barriers and forms R martensite via an isothermal fashion (path $b1$ of strain glass R). At just several kelvin below M_s (e.g., temperature T_2) where the driving force of R and $B19'$ increases, both R and $B19'$ will coexist [see Fig. 1(c)]. Far below M_s (e.g., temperature T_3), $B19'$ becomes more stable than R, which leads to normal observations (path a of strain glass $B19'$). (III) Figure 5(c) shows the effect of the Fe dopant (Ti$_{50}$Ni$_{48.7}$Fe$_{1.3}$). The competition also exists but Fe strongly stabilizes R martensite while creating weaker local barriers. Therefore, the system can overcome local barriers and form R martensite with fast kinetics (i.e., during continuous cooling). With further cooling, the R martensite transforms into the more stable $B19'$. (IV) Figure 5(d) shows the effect of Ti$_3$Ni$_4$ precipitates on the free energy landscape. These rhombohedral precipitates (formed by high-temperature aging of Ni-rich Ti-Ni alloys) produce favorable local strain for R martensite and thus stabilize R martensite while creating weak local barriers. For the same reason as the Fe-doping case, the system can form R martensite under continuous cooling.

A similar effect also holds for R-phase formation in transformation-cycled or cold-rolled Ti-Ni samples (with a high density of dislocations that provide a suitable stress field). Therefore, Fig. 5 provides a qualitative explanation for all-known situations of R-martensite formation. A quantitative modeling will appear elsewhere [23].

In conclusion, we have discovered a stable R phase existing in the Ti-Ni solid solution. It is the product of "crystallization" of strain glass, i.e., the growth of a SRO R phase with time. The experimental finding of the R phase supports theoretical predictions of its occurrence [21] and may stimulate further studies on the $B2$–$B19'$ transformation path of Ti-Ni alloys. The mechanism of crystallization of stain glass provides an alternative routine (varying time instead of varying temperature) to find phases and novel properties in martensitic systems and phase diagrams, which may lead to rich consequences as proved in diffusive systems and phase diagrams. Our work also suggests a practical classification for all isothermal martensite formations: a nucleation-controlled isothermal martensite formation or a growth-controlled isothermal martensite formation, which may help to clarify the complexity of isothermal martensitic transformations and to further reveal the nature.

---

[*]Corresponding author.
jiyuanchao@stu.xjtu.edu.cn
[†]dingxd@mail.xjtu.edu.cn
[‡]Xiaobing@nims.go.jp

[1] J. W. Christian, *The Theory of Transformations in Metals and Alloys* (Pergamon, Oxford, England, 2002).
[2] W. D. Callister, Jr., *Materials Science and Engineering: An Introduction*, 5th ed. (John Wiley & Sons, Inc., New York, 1999).
[3] A. G. Khachaturyan, *Theory of Structural Transformation in Solids* (John Wiley & Sons, Inc., New York, 1983).
[4] N. N. Thadhani and M. A. Meyers, Prog. Mater. Sci. **30**, 1 (1986).
[5] A. Planes, F. J. Perez-Reche, E. Vives, and L. Manosa, Scr. Mater. **50**, 181 (2004).
[6] L. Muller, U. Klemradt, and T. R. Finlayson, Mater. Sci. Eng. A **438**–**440**, 122 (2006).
[7] L. Muller, M. Waldorf, C. Gutt, G. Grubel, A. Madsen, T. R. Finlayson, and U. Klemradt, Phys. Rev. Lett. **107**, 105701 (2011).
[8] N. Shankaraiah, K. P. N. Murthy, T. Lookman, and S. R. Shenoy, Phys. Rev. B **84**, 064119 (2011).
[9] T. Kakeshita, K. Kuroiwa, K. Shimizu, T. Ikeda, A. Yamagishi, and M. Date, Mater. Trans., JIM **34**, 423 (1993).
[10] S. Kustov, D. Salas, E. Cesari, R. Santamarta, and J. Van Humbeeck, Acta Mater. **60**, 2578 (2012).
[11] *Shape Memory Materials*, edited by K. Otsuka and C. M. Wayman (Cambridge University Press, Cambridge, England, 1998).
[12] K. Otsuka and X. Ren, Prog. Mater. Sci. **50**, 511 (2005).
[13] S. Sarkar, X. Ren, and K. Otsuka, Phys. Rev. Lett. **95**, 205702 (2005).
[14] X. Ren, in *Disorder and Strain-induced Complexity in Functional Materials*, edited by T. Kakeshita, T. Fukuda, A. Saxena, and A. Planes (Springer, Berlin, 2012), Vol. 148.
[15] Z. Zhang, Y. Wang, D. Wang, Y. Zhou, K. Otsuka, and X. Ren, Phys. Rev. B **81**, 224102 (2010).
[16] Y. Ji, X. Ding, T. Lookman, K. Otsuka, and X. Ren, Phys. Rev. B **87**, 104110 (2013).
[17] E. Donth, *The Glass Transition: Relaxation Dynamics in Liquids and Disordered Materials* (Springer, Berlin, 2001).
[18] D. Wang, Z. Zhang, J. Zhang, Y. Zhou, Y. Wang, X. Ding, Y. Wang, and X. Ren, Acta Mater. **58**, 6206 (2010).
[19] G. Airoldi, G. Carcano, G. Riva, and M. Vanelli, J. Phys. IV (France) **05**, C2-281 (1995).
[20] See Supplemental Material at http://link.aps.org/supplemental/10.1103/PhysRevLett.114.055701 for determining the composition range of isothermal R martensite in the phase diagram.
[21] K. Parlinski and M. Parlinska-Wojtan, Phys. Rev. B **66**, 064307 (2002); P. Souvatzis, D. Legut, O. Eriksson, and M. I. Katsnelson, Phys. Rev. B **81**, 092201 (2010).
[22] T. Fukuda, T. Kakeshita, H. Houjoh, S. Shiraishi, and T. Saburi, Mater. Sci. Eng. A **273**–**275**, 166 (1999).
[23] D. Wang, Y. Ji, X. Ding, K. Otsuka, and X. Ren (to be published).